Evolution of Deformation and Recrystallization Textures in High-Purity Ni and the Ni-5 at. pct W Alloy

PINAKI P. BHATTACHARJEE, RANJIT K. RAY, and NOBUHIRO TSUJI

An attempt has been made to study the evolution of texture in high-purity Ni and Ni-5 at. pct W alloy prepared by the powder metallurgy route followed by heavy cold rolling (~95 pct deformation) and recrystallization. The deformation textures of the two materials are of typical pure metal or Cu-type texture. Cube-oriented ($\{001\}\langle 100\rangle$) regions are present in the deformed state as long thin bands, elongated in the rolling direction (RD). These bands are characterized by a high orientation gradient inside, which is a result of the rotation of the cube-oriented cells around the RD toward the RD-rotated cube ($\{013\}\langle 100\rangle$). Low-temperature annealing produces a weak cube texture along with the $\{013\}\langle 100\rangle$ component, with the latter being much stronger in high-purity Ni than in the Ni-W alloy. At higher temperatures, the cube texture is strengthened considerably in the Ni-W alloy; however, the cube volume fraction in high-purity Ni is significantly lower because of the retention of the $\{013\}\langle 100\rangle$ component. The difference in the relative strengths of the cube, and the $\{013\}\langle 100\rangle$ components in the two materials is evident from the beginning of recrystallization in which more $\{013\}\langle 100\rangle$-oriented grains than near cube grains form in high-purity Ni. The preferential nucleation of the near cube and the $\{013\}\langle 100\rangle$ grains in these materials seems to be a result of the high orientation gradients associated with the cube bands that offer a favorable environment for early nucleation.

DOI: 10.1007/s11661-010-0345-9

I. INTRODUCTION

THE development of a strong cube texture ($\{001\}\langle 100\rangle$) in medium-to-high stacking fault energy face-centered cubic (fcc) materials, after heavy cold rolling and recrystallization, has received a lot of attention. The origin of cube texture is particularly interesting because, although a strong cube component is present in the recrystallization texture, no significant presence of the cube usually is found in the deformed state, as revealed from macroscopic pole figure or orientation distribution function (ODF) analyses. To resolve this apparent anomaly, two competing theories have been proposed, namely the oriented nucleation and the oriented growth theories.[1] The oriented nucleation theory maintains that cube grains will nucleate from the deformed state more frequently than grains of other orientations. Obviously, the cube grains will nucleate from the preexisting cube-oriented regions in the deformed matrix. In contrast, the oriented growth theory emphasizes that the origin of sharp cube texture lies in the selective growth of the nucleated cube grains. The oriented growth theory is mainly based on the observations that certain misorientation relationships such as 40 deg around $\langle 111\rangle$ can have a high mobility, and such a high mobility relationship is, in fact, found to hold well between the cube component and variants of the S-orientation ($\{123\}\langle 634\rangle$), which is one of the main components of deformation texture in many medium-to-high stacking fault energy fcc materials. The origin of the preexisting cube-oriented regions and the reason for their preferential nucleation as maintained in the oriented nucleation model is not yet clear. It has been argued that the preexisting cube regions in the deformed matrix could originate by a rotational mechanism,[2] or they could be the remnants of the original cube-oriented grains existing in the hot-rolled materials.[3,4]

The current work deals with the development of cube texture in high-purity Ni and Ni-5 at. pct W alloy prepared by powder metallurgy (PM) followed by heavy cold rolling and recrystallization. The understanding of the development of cube texture in these materials is critical for their intended use as a mechanically strong and textured substrate for coated superconductor applications according to the rolling assisted biaxially textured substrates method.[5] The substrate materials to be used for such applications should have a sharp cube texture in the recrystallized condition, as the presence of other orientations can introduce high-angle grain boundaries (HAGBs) in the substrate that are detrimental for achieving high critical current densities in the superconductor layers grown epitaxially on these substrates.[6] Although several studies have been carried out for optimizing the volume of cube texture in the Ni-W

PINAKI P. BHATTACHARJEE, Assistant Professor, is with the Department of Materials Science and Engineering, Indian Institute of Technology Hyderabad, Ordinance Factory Estate, Yeddumailaram 502205, India. Contact e-mail: pinakib@iith.ac.in RANJIT K. RAY, Visiting Scientist, is with the R&D Division, TATA Steel, Jamshedpur 831 001, India. NOBUHIRO TSUJI, Professor, is with the Department of Materials Science & Engineering, Graduate School of Engineering, Kyoto University, Yoshida Honmachi, Sakyo-ku, Kyoto 606-8501, Japan.

Manuscript submitted October 7, 2009.
Article published online July 7, 2010

alloy, the effect of W on the development of cube texture in high-purity Ni has not been clarified fully yet. Indications have emerged recently that W actually may enhance the formation of cube texture in high-purity Ni.[7,8] Thus, a detailed comparative study seems necessary at this juncture to identify the differences in the evolution of cube texture in high-purity Ni and Ni-W alloy systems. In the current work, an attempt has been made to clarify the origin of the sharp cube texture in powder metallurgically prepared high-purity Ni and Ni-W alloy *vis à vis* the role of W on enhancing the cube texture in Ni, with particular emphasis on the deformation structures of high-purity Ni and Ni-W alloy. In general, the development of cube texture has been studied mostly in materials prepared by the conventional melting and casting route. Studies pertaining to the development of cube texture in materials prepared by PM are limited in comparison presumably because PM is a near net shape method of production in which further deformation processing is not common. However, the PM materials in the sintered condition (starting materials for subsequent deformation processing) are expected to have a different microstructure and texture as compared with hot-rolled materials, and thus, the development of cube texture after heavy cold rolling and recrystallization in these materials could provide new insights into the origin of cube texture.

II. EXPERIMENTAL METHODS

A. *Processing*

The materials used for the current investigation were prepared by conventional PM route. To prepare the Ni-5 at. pct W alloy, elemental powders of high-purity Ni (99.99 pct purity; acquired from Sigma-Aldrich, St. Louis, MO) and W (99.6 pct, acquired from Teledyne Advanced Materials, Huntsville, AL) first were mixed in appropriate proportion. Loose powder mixes then were compacted by uniaxial pressing at 250 MPa. This process was followed by sintering of the green compacts at 1373 K (1100 °C) in flowing H_2 atmosphere. The sintered compacts of high-purity Ni and Ni-W alloy subsequently were cold rolled to ~95 pct deformation corresponding to a final thickness close to ~150 μm. The rolling was done in a laboratory-scale rolling mill with oil-lubricated rolls having 150-mm diameter. During the cold rolling, 10 pct to 15 pct thickness reduction per pass was used. All cold-rolled tapes were subjected to annealing treatment to study the recrystallization texture development. For this purpose, small pieces of cold-rolled sheets were vacuum sealed (~10^{-5} torr) in a quartz tube to prevent oxidation and were subjected to heat treatment in a vertical tube furnace. The controller attached to the furnace was capable of maintaining the temperature within a range of ± 5 °C. For high-purity Ni, the annealing temperatures were 773 K (500 °C), 1073 K (800 °C), and 1373 K (1100 °C), and for the Ni-W alloy, the annealing temperatures were 1073 K (800 °C), 1373 K (1100 °C), and 1523 K (1250 °C). The annealing time was one hour in all cases. In addition, to monitor the evolution of the different recrystallization texture components in high-purity Ni and Ni-W alloy, the two materials were annealed at 573 K (300 °C) and 973 K (700 °C), respectively, for various lengths of time. All heat-treated samples subsequently were quenched in cold water.

B. *Characterization*

Macroscopic textures of the cold-rolled and fully recrystallized materials were measured by X-ray diffraction (XRD) with a Siemens D5000 X-ray texture Goniometer (Munich, Germany). For each material, four incomplete pole figures, {111}, {200}, {220}, and {311} were measured, and ODFs were calculated after correction and symmetrization using the series expansion method of Bunge[9] with a limit of $l_{max} = 22$. The volume fraction of a given texture component was determined within a spread of 15 deg around its ideal location in the Euler space. Microstructure and microtexture of the materials were determined by electron backscatter diffraction (EBSD) studies. For fully recrystallized materials, an EBSD system attached to a FEI- Quanta 200 scanning electron microscope (SEM) (Hillsboro, OR) (W filament gun type) was employed. Microtextures of the cold-rolled and partially recrystallized materials were studied by an automated EBSD system attached with an FEI-SIRION SEM equipped with a field emission gun (FEG). In all cases, TSL-OIM software was used for the analysis of the microtexture data. The samples for EBSD measurements were prepared by mechanical polishing followed by electropolishing at room temperature.

III. RESULTS

A. *Microstructure and Texture of the Starting Materials*

Figures 1(a) and (b) show the grain boundary (GB) maps obtained from the EBSD analysis of high-purity Ni and Ni-W alloy in the sintered condition. Figures 1(c) and (d) are the corresponding (111) pole figures. The normal direction (ND) in the pole figure is parallel to the direction of pressing. The HAGBs and low-angle grain boundaries ([LAGBs] having misorientation angle [$\theta_{mis} \geq 15$ deg] and [2 deg $\leq \theta_{mis} \leq 15$ deg], respectively) are shown as thin black and grey lines, respectively, in the GB maps. The clusters of black points (arrowed) in the microstructure of the Ni-W alloy (Figure 1(b)) are the residual pores after the sintering treatment. In comparison with high-purity Ni, the Ni-W alloy shows a higher pore fraction and also profuse annealing twins. The average grain sizes of the high-purity Ni and Ni-W alloy in the sintered condition, measured from the boundary maps by the liner intercept method (twins are not considered as separate grains for grain size measurement), are ~9 μm and 13 μm, respectively. The starting textures of the materials are weak, as may be judged by the appearance and intensities of the (111) pole figures of the two materials.

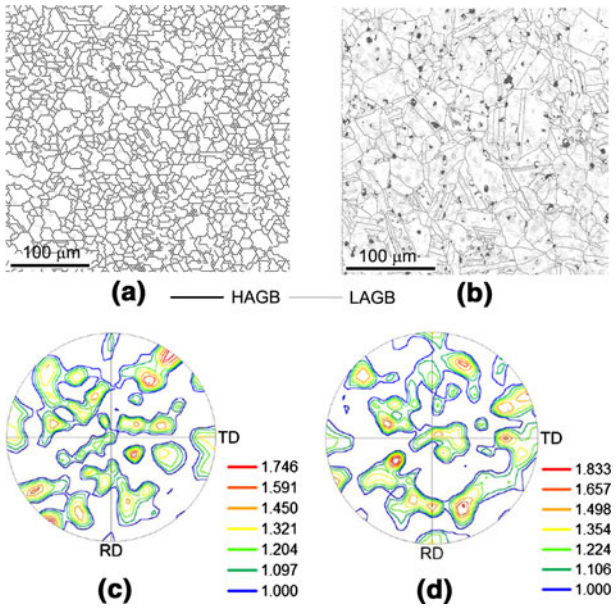

Fig. 1—(*a*) and (*b*) are the EBSD GB maps of high-purity Ni and the Ni-W alloy after sintering at 1373 K (1100 °C) for 1 h; (*c*) and (*d*) are the corresponding (111) pole figures.

B. *Deformed Condition*

1. *Macroscopic Texture Analyses*

Figures 2(a) and (b) show the (111) X-ray pole figures for the 95 pct cold-rolled high-purity Ni and Ni-W alloy, respectively. The pole figures are typical of heavily rolled medium-to-high stacking fault energy fcc materials. The volume fractions of typical deformation texture components in the two materials have been compared in the histogram in Figure 2(c). The volume fraction of the cube component is low and almost similar in the two materials (<1 pct). Compared with the Ni-W alloy, high-purity Ni shows higher volume fractions of the Cu, S, and Bs components. The volume fractions of the orientations that do not belong to any of the typical rolling texture components have been denoted as "others" in Figure 2(c). The combined volume fraction of these orientations is higher in the Ni-W alloy. Qualitative and quantitative analyses of the deformation textures of the two materials thus indicate that they do not differ significantly from each other, and the cold-rolling textures of the two materials could be classified as Cu type or pure metal type.

2. *Microtexture Analyses*

Microtexture studies were carried out on the deformed materials to identify the variations in microstructure and texture at a local scale. For this purpose, a number of EBSD scans were carried out from the ND-rolling direction (RD) section of the deformed materials.

Figure 3 shows the crystal orientation map of a region of interest in high-purity Ni. The HAGBs are shown as thin black lines in the map. The microstructure shown in Figure 3 is of a lamellar type, finely subdivided by HAGBs along the ND, and is typical of heavily deformed materials.[10,11] The analysis of the local texture of this region shown in the crystal orientation map indicates a significant presence of the Cu (red, 21 pct), S (yellow, 27 pct), Bs (green, 21 pct), and some amount of Goss (orange, 7 pct) orientations. In addition, a $\{013\}\langle 100\rangle$ orientation also has been highlighted in the map (purple). This orientation basically is obtained by ~19 deg rotation of the cube component around the RD ($\|\langle 100\rangle$). The component around $\{013\}\langle 100\rangle$ is addressed hereafter as the rotated cube. The significance of including this orientation will be discussed later in conjunction with the development of annealing textures. Cube-oriented regions (blue) appear as thin bands running parallel to the RD. It may be noted that inside the elongated cube band shown in Figure 3, the orientation changes from $\{013\}\langle 100\rangle$ on one side of the band to the $\{100\}\langle 001\rangle$ orientation at the other end of the band. The volume fraction of the rotated cube orientation is higher than that of the cube orientation (~3 pct and 0.6 pct, respectively).

The cube bands typically observed in this material are characterized by the presence of a high orientation gradient, which is not usually observed for bands of other orientations. This is illustrated in Figure 4. Figure 4(a) is the orientation map of a magnified region in Figure 3, and Figure 4(b) is the corresponding GB map. Several arrow marks have been included in the orientation map in Figure 4(a). Figure 4(c) shows the point-to-point and point-to-origin misorientations of the cube and along bands of several other orientations, as marked by the arrows. The point-to-point misorientation in all cases is low and is typical of cell misorientations, but the point-to-origin or the accumulated misorientations are comparatively large. Only for the cube band, the accumulated misorientation builds up to a rather large value (~25 deg) across a fairly small distance. For bands of other orientations, the accumulated misorientation either dips or levels off across small distances. It is shown in the GB map in Figure 4(b) that no high-angle boundaries are present inside the cube band (indicated by an arrow mark in Figure 4(b)). This indicates that the cube and the rotated cube belonged to the same deformed grain, and the orientation gradient inside the cube band is a result of the rotation of cube-oriented cells around the RD toward $\{013\}\langle 100\rangle$ orientation. It may be mentioned here that numerous cube bands found in this material show similar misorientation profiles, as depicted in Figure 4.

The microstructure of high-purity Ni obtained from several other EBSD scans seem to be somewhat similar to that shown in Figure 3. Large-scale deformation heterogeneities are encountered rarely in this material. However, for the Ni-W alloy, large variations in microstructure and texture are found between different regions owing to the presence of deformation heterogeneities.

Figure 5(a) shows the orientation map of a typical lamellar region in the ~95 pct deformed Ni-W alloy, and Figure 5(b) shows the corresponding GB map. This region is characterized by a negligible presence of the Cu component (red) as well as significant presence of the S orientation (~18 pct) (yellow) and some amount of B_s orientation (~7 pct) (green). Cube-oriented regions are present in thin bands along with the RD-rotated cube

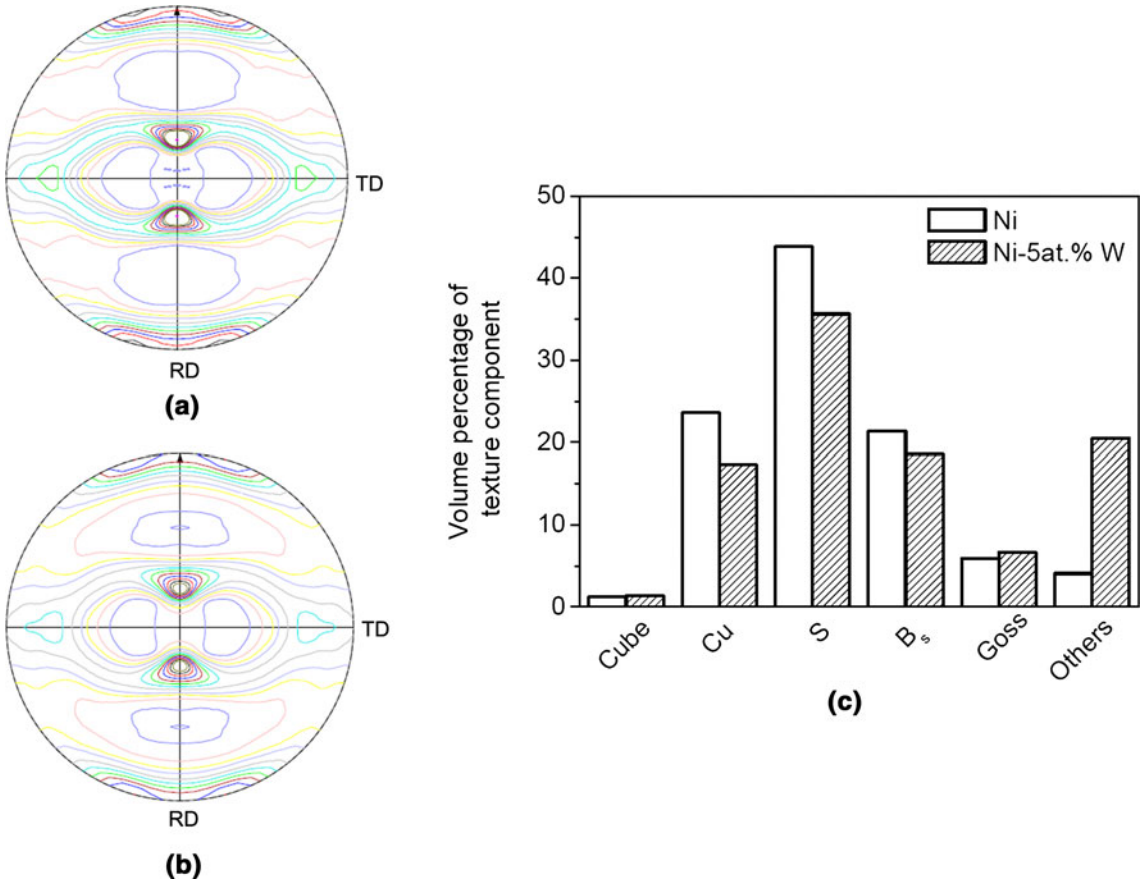

Fig. 2—(111) pole figures of 95 pct cold-rolled high-purity Ni and the Ni-W alloy determined by XRD; (*c*) shows the volume fractions of typical deformation texture components.

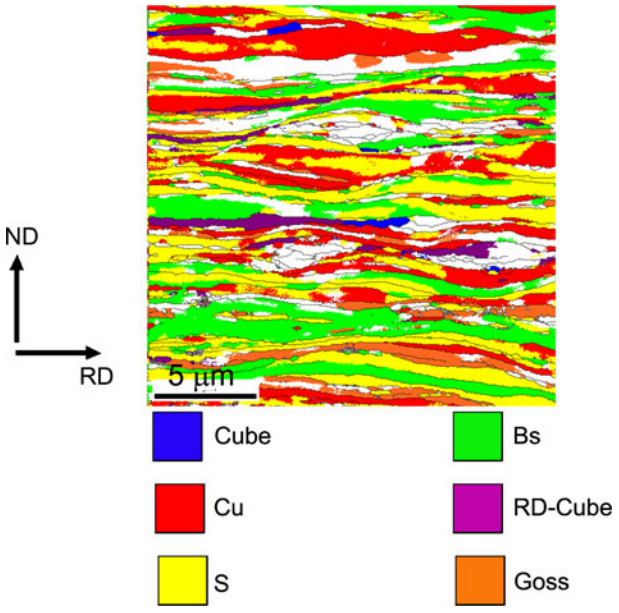

Fig. 3—(Color online) Orientation map of 95 pct cold-rolled high-purity Ni showing the distribution of typical rolling texture components. HAGBs are highlighted in black lines in the map.

orientation, and the cube fraction is decidedly more than that obtained from the bulk texture analysis. However, the volume fraction of the RD-rotated cube orientation is more than that of the near cube orientation in this region. The point-to-point and point-to-origin misorientations along the arrow marks in Figure 5(a) for cube, S, and "other" orientation bands have been shown in Figure 5(c). The point-to-point misorientation is low in all cases, but the point-to-origin misorientation accumulates to a high value for the cube band in contrast to bands of other orientations. These observations are apparently similar to those made for high-purity Ni (Figure 4), although some subtle differences will be pointed out in the discussion. As for the cube band observed in high-purity Ni, no high-angle boundaries could be observed inside the cube band in the Ni-W alloy, as indicated by the arrow mark in the GB map in Figure 5(b). Thus, here too, the cube and the rotated cube orientations belonged to the same deformed grain, and the orientation gradient inside the cube band is a result of the rotation of the cube around the RD toward the $\{013\}\langle 100\rangle$ orientation. This misorientation profile along the cube bands is similar in a large number of such bands. Thus, this seems to be a general behavior of cube bands in this material.

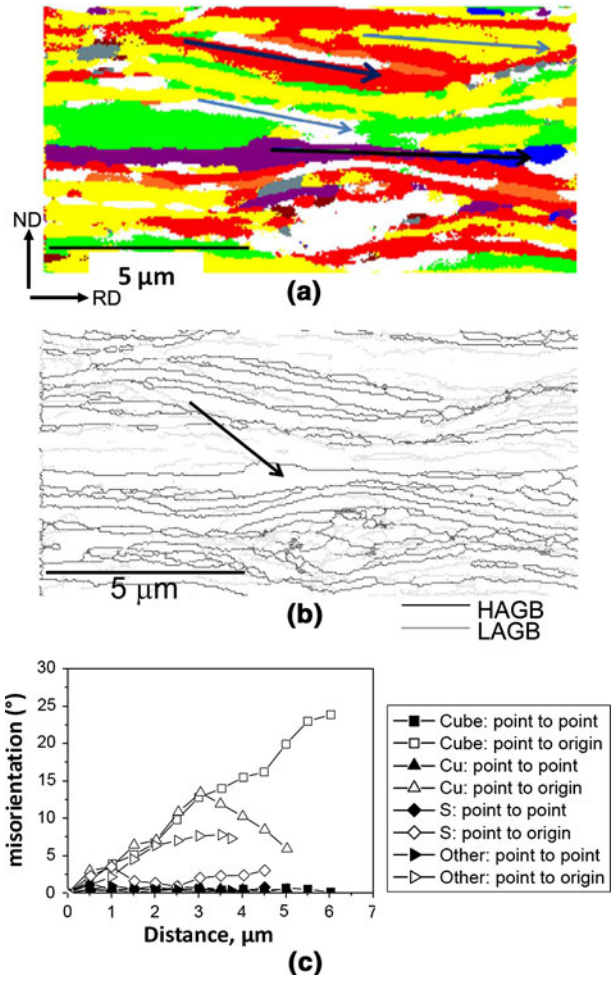

Fig. 4—(Color online) (*a*) Orientation map of a selected region in Fig. 3; (*b*) the corresponding GB map; (*c*) misorientation *vs* distance plot for different orientation bands recorded along the respective arrow marks in (*a*) for different bands. The color codes for the orientation map are the same as in Fig. 3.

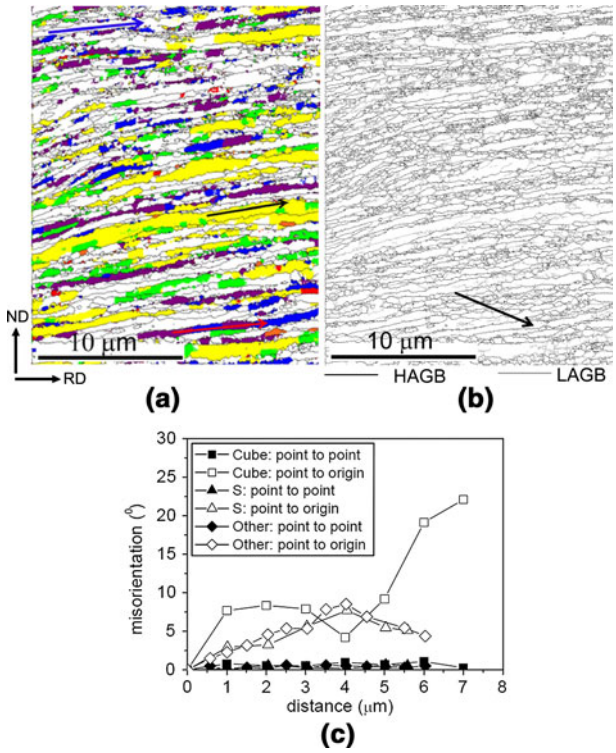

Fig. 5—(*a*) Orientation map for the deformed Ni-W alloy (color key is the same as in Fig. 3); (*b*) the corresponding GB map; (*c*) misorientation *vs* distance plot for different orientation bands recorded along the respective arrow marks in (*a*) for different bands.

Figures 6(a) and (b) show the orientation maps of a few selected regions in the deformed Ni-W alloy that have experienced localized shearing. The differences in the microtextures of these regions with those of the lamellar regions have been shown quantitatively in the histogram in Figure 7. The deformation textures in the locally sheared regions are generally weak and different from that obtained from the macroscopic X-ray texture. The presence of weak texture in these regions as compared with the lamellar regions is reflected in the large volume fractions associated with the ''other'' orientations.

3. *Annealed Condition*

Figure 8(a) shows the $\Phi_2 = 0$ deg section of the ODF (determined by EBSD) of high-purity Ni after annealing at 773 K (500 °C) for 1 hour. The average size of the recrystallized grains in this condition is ~11 μm (determined from the EBSD maps by linear intercept methods). The ODF indicates the development of cube texture, but this is not sharp at this stage, and a noticeable spread of the cube component around the RD (manifested by shift of the intensity maxima about Φ) is shown, which indicates the development of a strong rotated cube orientation. To obtain the location of the intensity maxima associated with the rotated cube component, the cube-oriented grains first are excluded from the original data set, and the ODF is calculated again from the off-cube grains only (>15 deg misorientation with exact cube orientation). Figure 8(b) shows the $\Phi_2 = 0$ deg section calculated from the off-cube dataset. The location of the intensity maxima is shifted ~19 deg from the exact cube toward the Goss location, which is near $\{013\}\langle100\rangle$. The orientation map corresponding to this 773 K (500 °C) annealed condition is shown in Figure 8(c). Two additional texture components besides those listed in Figure 3, namely, $\{221\}\langle122\rangle$ and $\{185\}\langle221\rangle$ have been shown in grey and dark red colors, respectively. These two components are the twin related orientations of the cube and the $\{013\}\langle100\rangle$ orientation, respectively. The volume fraction of the cube component in this condition is ~14 pct, while that of the rotated cube component is almost twice this value at ~26 pct.

The orientation maps of the high-purity Ni alloy after annealing at 1073 K (800 °C) and 1373 K (1100 °C) for 1 hour are shown in Figures 9(a) and (b), respectively. The average grain sizes in these two recrystallized conditions are ~28 μm and ~80 μm, respectively. The volume fractions of the cube component has increased to ~26 pct after annealing at 1073 K (800 °C), but the rotated cube component (~32 pct) is still stronger than

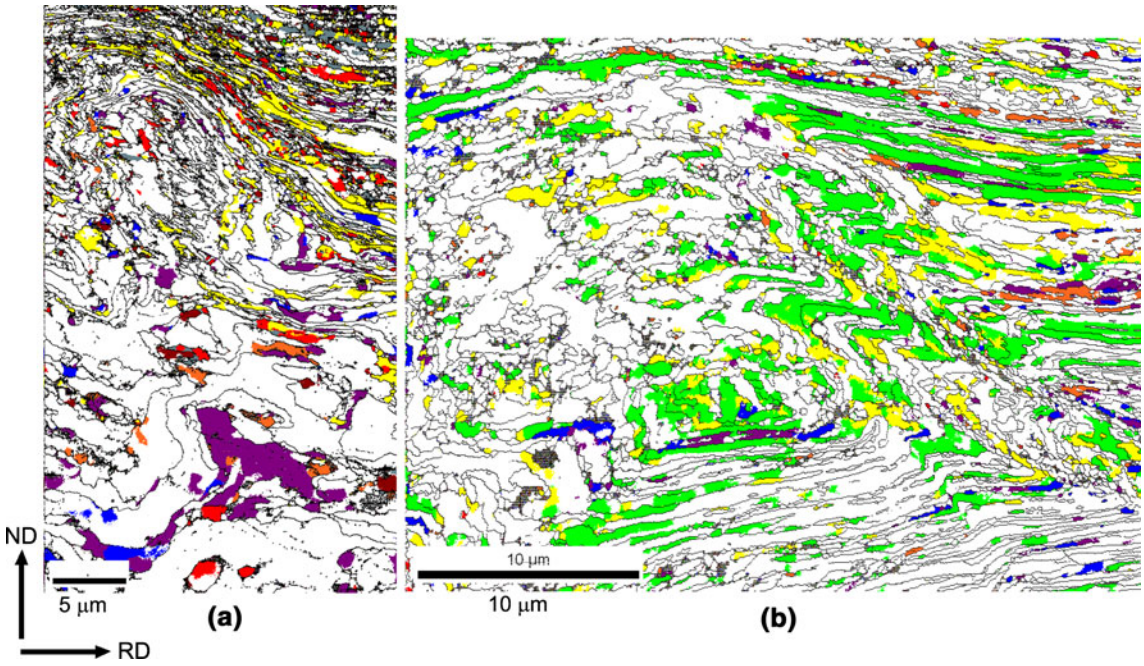

Fig. 6—(Color online) (*a*) and (*b*) are the orientation maps showing regions in the ~95 pct cold-rolled Ni-W alloy undergoing localized shearing. Color codes are the same as in Fig. 3.

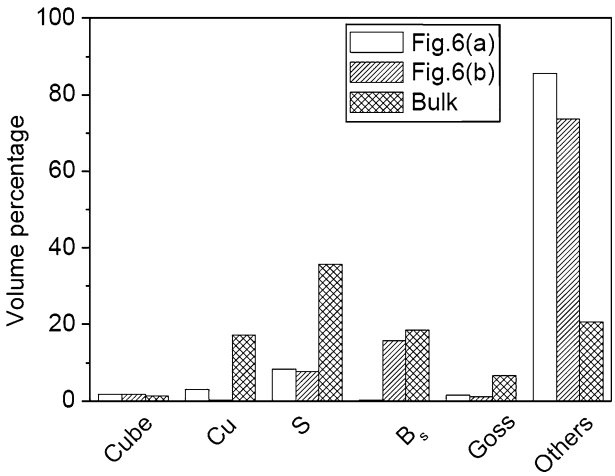

Fig. 7—Comparison of microtexture in localized sheared regions in Figs. 6(a) and (b) with the lamellar regions.

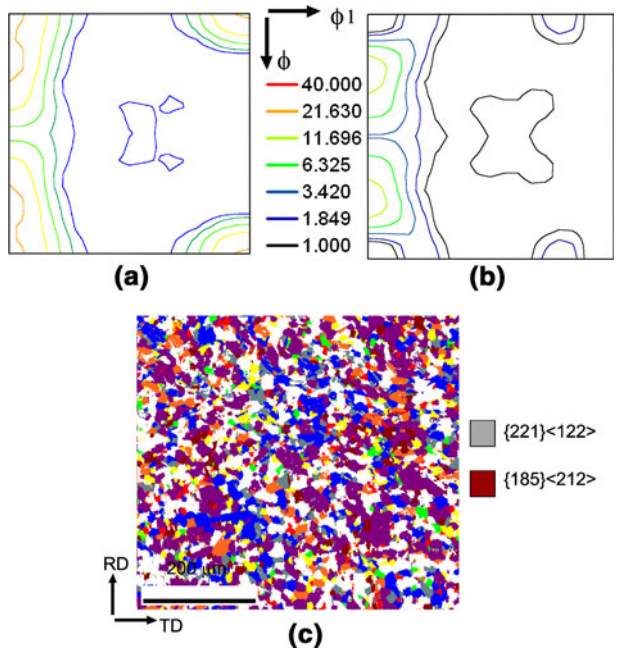

Fig. 8—(Color online) Φ_2 = 0 deg section of the ODF (obtained from EBSD) of ~95 pct cold-rolled high-purity Ni after annealing at 773 K (500 °C) calculated from (*a*) all orientations and (*b*) off-cube orientations only. (*c*) is the orientation map in this recrystallized condition. Color codes are the same as in Fig. 3, except for the two orientations {221}⟨122⟩ and {185}⟨212⟩.

the cube component. After annealing at 1373 K (1100 °C), the cube fraction increases to ~50 pct, presumably at the expense of the grains of other noncube orientations. A significant presence of the rotated cube orientation still could be observed, but the volume fraction (~27 pct) has decreased as compared with the 1073 K (800 °C) annealed condition.

Figure 10(a) shows the Φ_2 = 0 deg section of the ODF of the Ni-W alloy after annealing at 1073 K (800 °C) for 1 hour. The existence of the rotated cube component alongside the cube component is shown in the Φ_2 = 0 deg section of the ODF, which is calculated from the off-cube grains (Figure 10(b)) in a manner similar to that for the high-purity Ni (Figure 8(b)). The volume fraction of the cube component in this condition is ~14 pct and that of the rotated cube grains is ~11 pct. The average grain size in this condition is ~8 μm.

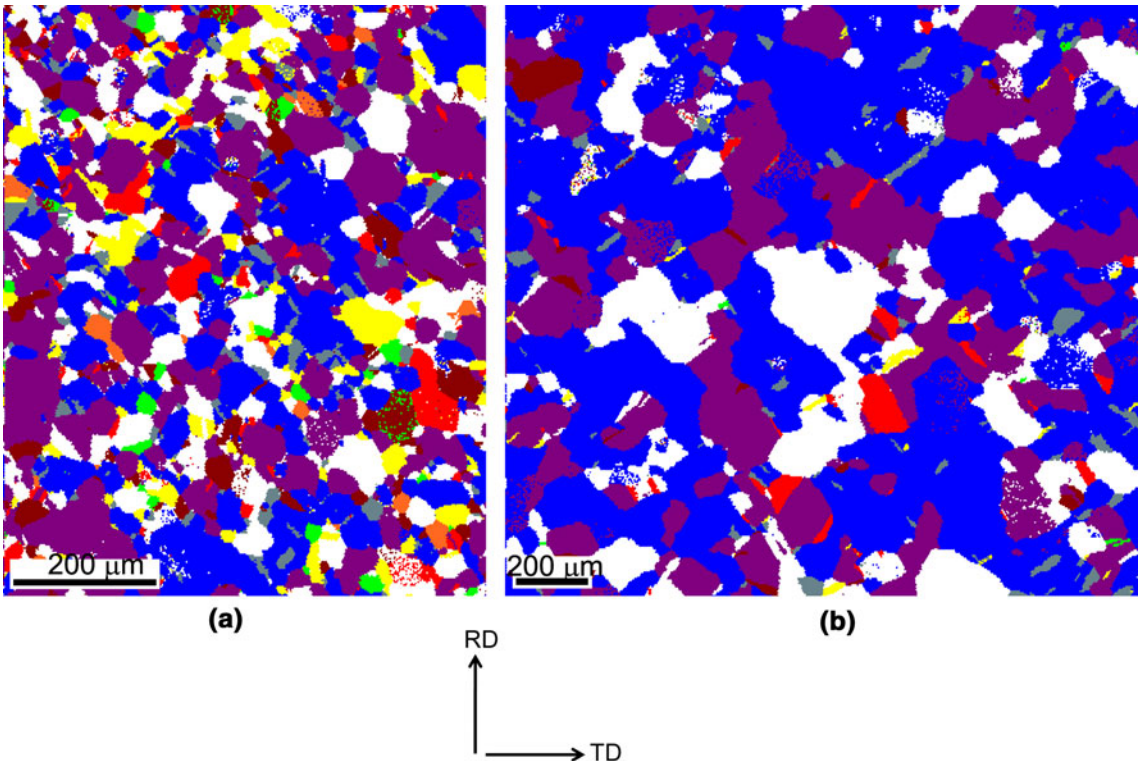

Fig. 9—(Color online) Orientation maps of the ~95 pct cold-rolled high-purity Ni annealed at (*a*) 1073 K (800 °C) and (*b*) 1373 K (1100 °C). The color key of the orientation map is the same as in Fig. 8.

The orientation maps of Ni-W alloy after annealing at 1373 K (1100 °C) and 1523 K (1250 °C) are shown in Figures 11(a) and (b), respectively. The average grain sizes in these two annealed conditions are ~25 μm and ~75 μm, respectively. The cube and rotated cube volume fractions are ~62 pct and ~15 pct, respectively, after annealing at 1373 K (1100 °C). The cube volume fraction increases to ~80 pct, whereas the rotated cube fraction decreases to ~12 pct after annealing at 1523 K (1250 °C). Figure 12 summarizes the volume fractions of the cube and the rotated cube component after various annealing treatments.

C. *Nucleation of Recrystallization and Formation of Recrystallization Textures*

To investigate the process of nucleation and the formation of cube texture in the two materials, the high-purity Ni and the Ni-W alloy were annealed at 573 K (300 °C) and 973 K (700 °C), respectively, for various lengths of time. The time duration was adjusted so that a similar average recrystallized fraction is obtained in the two materials after the heat treatments. The recrystallized fraction varied greatly between different EBSD scans, particularly at the early recrystallization stage. Many times, recrystallized grains were clustered together in some areas at this stage. Thus, for statistical accuracy, the data of EBSD scans obtained from several regions were merged together, and the recrystallized volume fraction and texture were calculated from the combined dataset. However, only a few selected scans would be shown here that adequately represent the recrystallized state and texture. The recrystallized volume fractions chosen for this purpose were ~10 pct, 60 pct, and 100 pct corresponding to the early, intermediate, and fully recrystallized conditions, respectively. The recrystallized regions were separated from the deformed regions applying a set of criteria, namely internal misorientation, grain size, and neighborhood misorientation. Recrystallized grains are those regions that have internal misorientation (termed kernel average misorientation in the TSL-OIM software used in this analysis[12]) less than 1.5 deg and grain size (in area) larger than 4 μm^2. The regions selected in this way were checked further to find whether they are separated from their neighboring regions by HAGBs across a substantial part of their length. A set of similar criteria also have been employed by Li *et al.*[13] to separate the recrystallized regions from the deformed regions in partially recrystallized high-purity Ni.

Figure 13 shows the early recrystallization stage (annealed at 573 K (300 °C) for 300 seconds) in high-purity Ni, corresponding to an average recrystallized volume fraction of ~14 pct. Figures 13(a) and (b) are the orientation maps of typical regions in the partially recrystallized material, and Figures 13(c) and (d) are the corresponding orientation maps showing the recrystallized fractions only. The orientation maps indicate the presence of more rotated cube regions than near cube regions in this early recrystallized condition. This is further demonstrated in the $\Phi_2 = 0$ deg section of the discrete ODF plot in Figure 13(e).

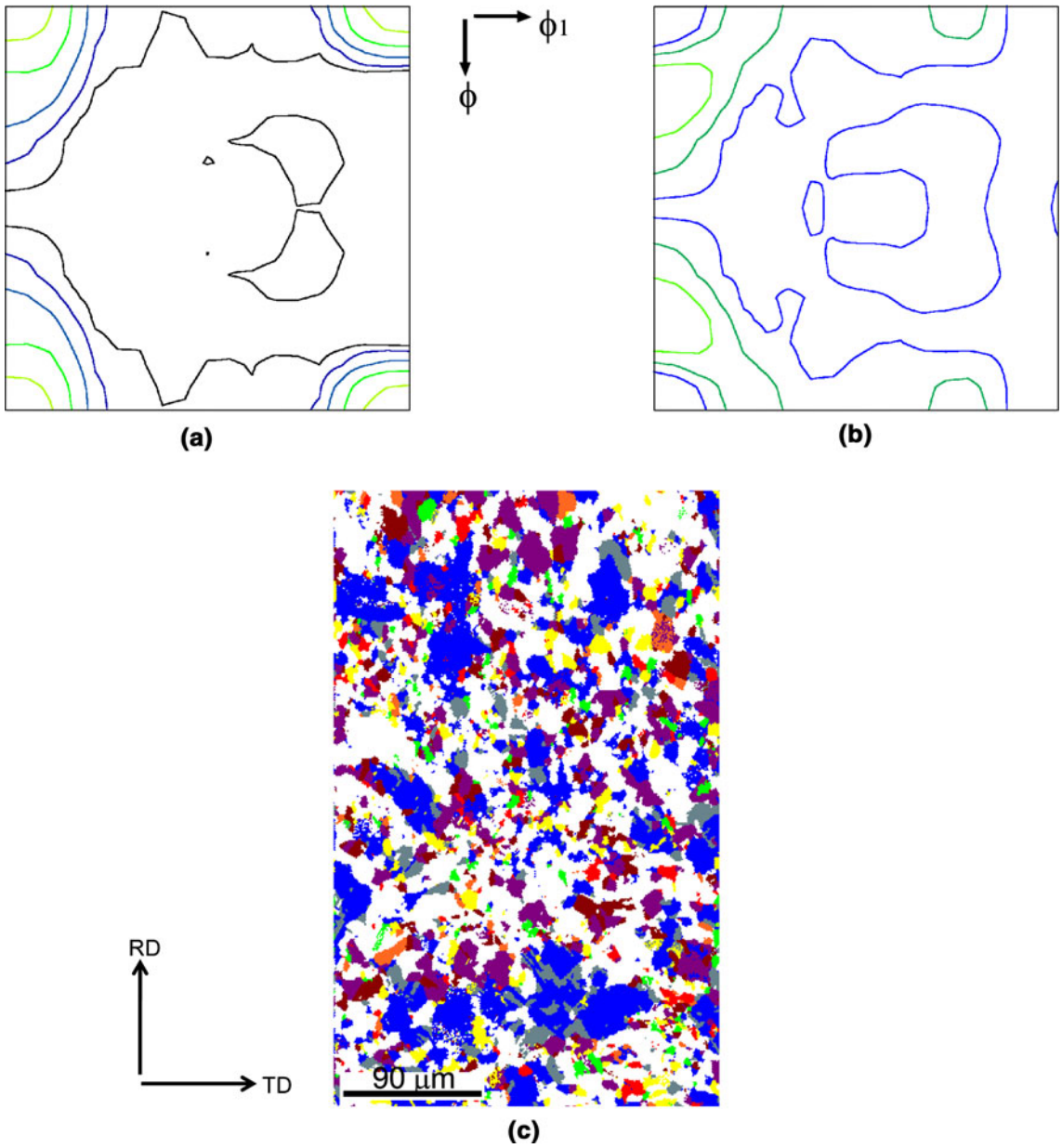

Fig. 10—(Color online) Φ_2 = 0 deg section of the ODF of the ~95 pct cold-rolled Ni-W alloy after annealing at 1073 K (800 °C) calculated from (*a*) all orientations and (*b*) off-cube orientations only. (*c*) The orientation map in this recrystallized condition. The color key of the orientation map is the same as in Fig. 8.

Figure 14 shows the early recrystallization stage in the Ni-W alloy obtained after annealing at 973 K (700 °C) for 225 seconds. The average recrystallized fraction in this condition is ~15 pct. Figures 14(a) and (b) are the orientation maps that include both deformed and recrystallized regions, whereas Figures 14(c) and (d) are the corresponding orientation maps showing the recrystallized regions only. Figure 14(c) shows many recrystallized grains, whereas few recrystallized grains can be identified in Figure 14(d), indicating the heterogeneous nature of nucleation of recrystallization. In sharp contrast to high-purity Ni, many cube-oriented grains can be identified in the orientation maps along with the presence of few rotated cube grains. This also can be understood clearly from the Φ_2 = 0 deg section of the discrete ODF plot in Figure 14(e).

A comparison between these early recrystallization stages in the two materials on a quantitative basis is shown in Figure 15, which indicates the number fractions of the differently oriented grains in the two materials. The number fraction of cube and rotated cube grains taken together does not differ to any significant extent in the two materials. However, the relative fractions of cube and rotated cube grains are different in the two materials. High-purity Ni shows more rotated cube grains than near cube grains, whereas the situation is just the opposite in the Ni-W alloy.

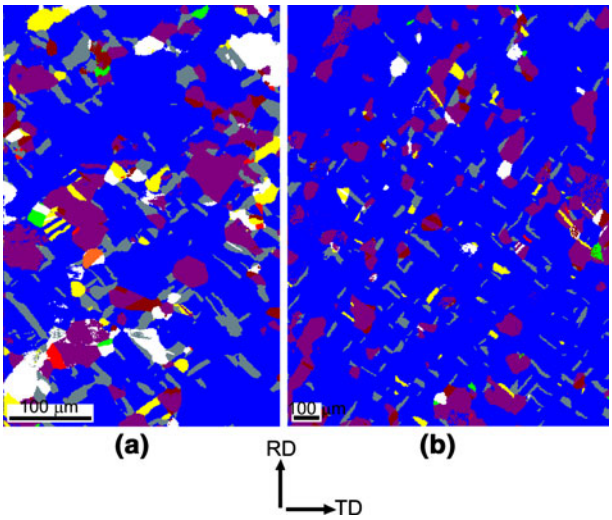

Fig. 11—(Color online) Orientation maps of ~95 pct cold rolled Ni-W alloy annealed at (*a*) 1373 K (1100 °C) and (*b*) 1523 K (1250 °C). The color key of the orientation map is the same as in Fig. 8.

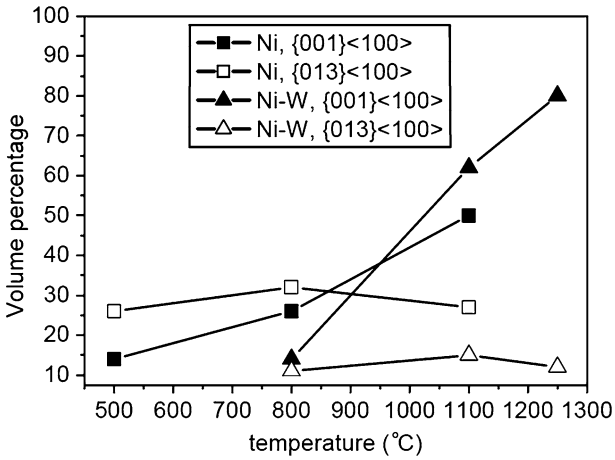

Fig. 12—Volume fractions of a cube and a rotated cube obtained after different annealing treatments in ~95 pct cold-rolled high-purity Ni and Ni-W alloy.

Figure 16 shows the changes in texture with progressive recrystallization in the two materials. These recrystallized conditions correspond to recrystallized volume fractions of ~60 pct and 100 pct (fully recrystallized condition), which are attained after 3 hours and 12 hours annealing at 573 K (300 °C) for high-purity Ni, and after 300 seconds and 600 seconds annealing at 973 K (700 °C) for the Ni-W alloy. Figures 16(a) and (b) are the $\Phi_2 = 0$ deg sections of the ODFs for high-purity Ni and the Ni-W alloy, respectively, at the intermediate recrystallized condition (~60 pct recrystallized). Figures 16(c) and (d) are the $\Phi_2 = 0$ deg sections of the ODFs for high-purity Ni and the Ni-W alloy, respectively, after complete recrystallization. At the intermediate recrystallized condition, the spread of the cube component around the RD is evident in the ODF of high-purity Ni (Figure 16(a)). The cube component is sharper in the Ni-W alloy, which also shows the presence of more near cube-oriented regions than rotated cube regions (Figure 16(b)). These characteristics of the recrystallization texture in the two materials correspond well with the texture in the early recrystallization stage. On completion of recrystallization, the spread of the cube component around the RD is strongly retained in high-purity Ni (Figure 16(c)), indicating the development of a strong rotated cube component along with the cube component. The $\Phi_2 = 0$ deg section of the Ni-W alloy in the fully recrystallized condition, in contrast, indicates a significantly less spread of the cube component and a weaker rotated cube component (Figure 16(d)).

IV. DISCUSSION

The results of the current study show that high-purity Ni and the Ni-W alloy develop different recrystallization textures, although the deformation textures of the two materials seem similar. After annealing at low temperatures, a diffuse cube texture develops in the two materials accompanied by a rotated cube component. The rotated cube component is, however, much stronger in high-purity Ni than in the Ni-W alloy. Remarkable difference in the strength of the cube texture, however, is observed in the two materials after high-temperature annealing. The Ni-W alloy develops a much stronger cube texture than high-purity Ni. In high-purity Ni, the rotated cube component is retained even after high-temperature annealing, which diminishes the strength of the cube component.

It further is observed that the cube-oriented regions in the form of extended cube bands are present in the deformed microstructures of both high-purity Ni and the Ni-W alloy. These bands involve a difference of orientation from the near cube $\{001\}\langle100\rangle$ to the rotated cube $\{013\}\langle100\rangle$ orientation from one end of the band to the other, which results in a high-orientation gradient inside the cube bands. In both high-purity Ni and the Ni-W alloy, the volume fraction of the $\{013\}\langle100\rangle$ orientation is higher than that of the near cube $\{001\}\langle100\rangle$ in the deformed condition. The early recrystallized grains in the two materials, however, show markedly different orientations. In the early stages of recrystallization, high-purity Ni shows more $\{013\}\langle100\rangle$ recrystallized grains than near $\{001\}\langle100\rangle$ grains, whereas the situation is just the opposite in the Ni-W alloy, although the number fraction of the $\{013\}\langle100\rangle$ and $\{001\}\langle100\rangle$ recrystallized grains taken together does not differ significantly in the two materials.

We now will try to discuss the previous results in light of the known facts and observations on cube texture formation in fcc materials. The strong preference for the nucleation of the near cube and the rotated cube grains, as compared with other rolling texture components, and the overwhelming predominance of grains of these orientations after recrystallization is complete clearly indicate a strong oriented nucleation of the cube (and the rotated cube) grains. It has to be remembered that both the cube and the rotated cube orientations can be found in the two ends of the same cube band in many

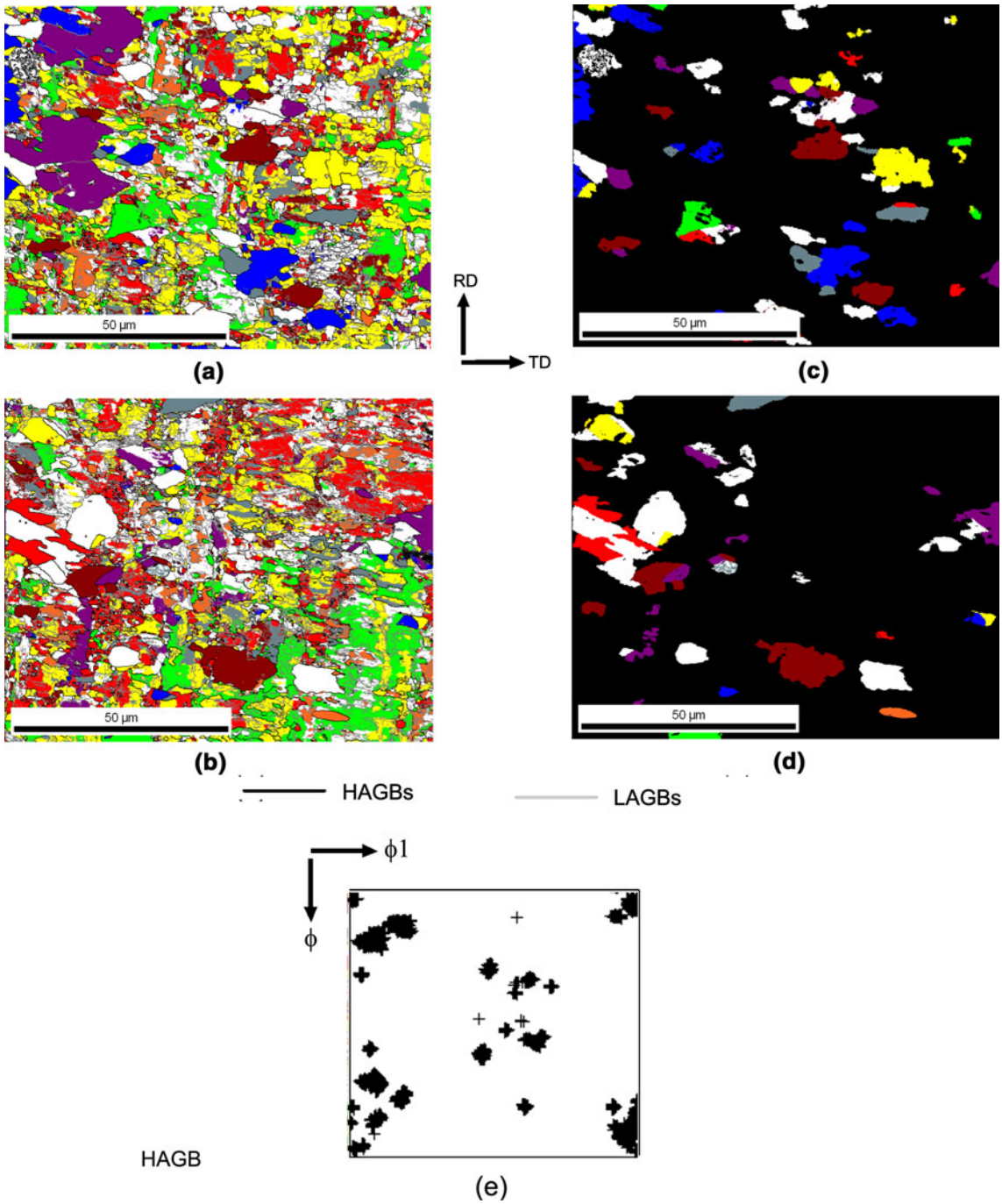

Fig. 13—(*a*) and (*b*) are orientation maps of ~95 pct cold-rolled high-purity Ni after partial recrystallization at 573 K (300 °C) for 300 s; (*c*) and (*d*) are orientation maps showing the recrystallized fraction only. (*e*) The $\Phi_2 = 0$ deg section of the discrete ODF plot compiled from the recrystallized fraction of several orientation maps.

cases. To nucleate, the potential nuclei (1) must acquire a critical size and (2) should be bounded by HAGBs. The stable size could be achieved by the formation of bulges by individual cube-oriented subgrains from the boundaries of the cube bands into the neighboring deformed matrix by a mechanism such as strain-induced boundary migration, as observed by Ridha and Hutchinson[14] in cold-rolled copper or by subgrain growth in an orientation gradient.[15] In the current case, the high-orientation gradient within the cube bands in the deformed materials offers a favorable environment for the nucleation of cube (and rotated cube) grains. Zaefferer *et al.*[15] in their investigation on cold-rolled Fe-36 wt pct Ni alloy also have observed that a high-orientation gradient exists within the cube bands and argued that the nucleation of cube grains inside the cube bands is energetically more favorable than nucleation by the formation of bulges by individual cells from the band boundaries, as this will involve a large radius of curvature. Nucleation through bulge formation has not

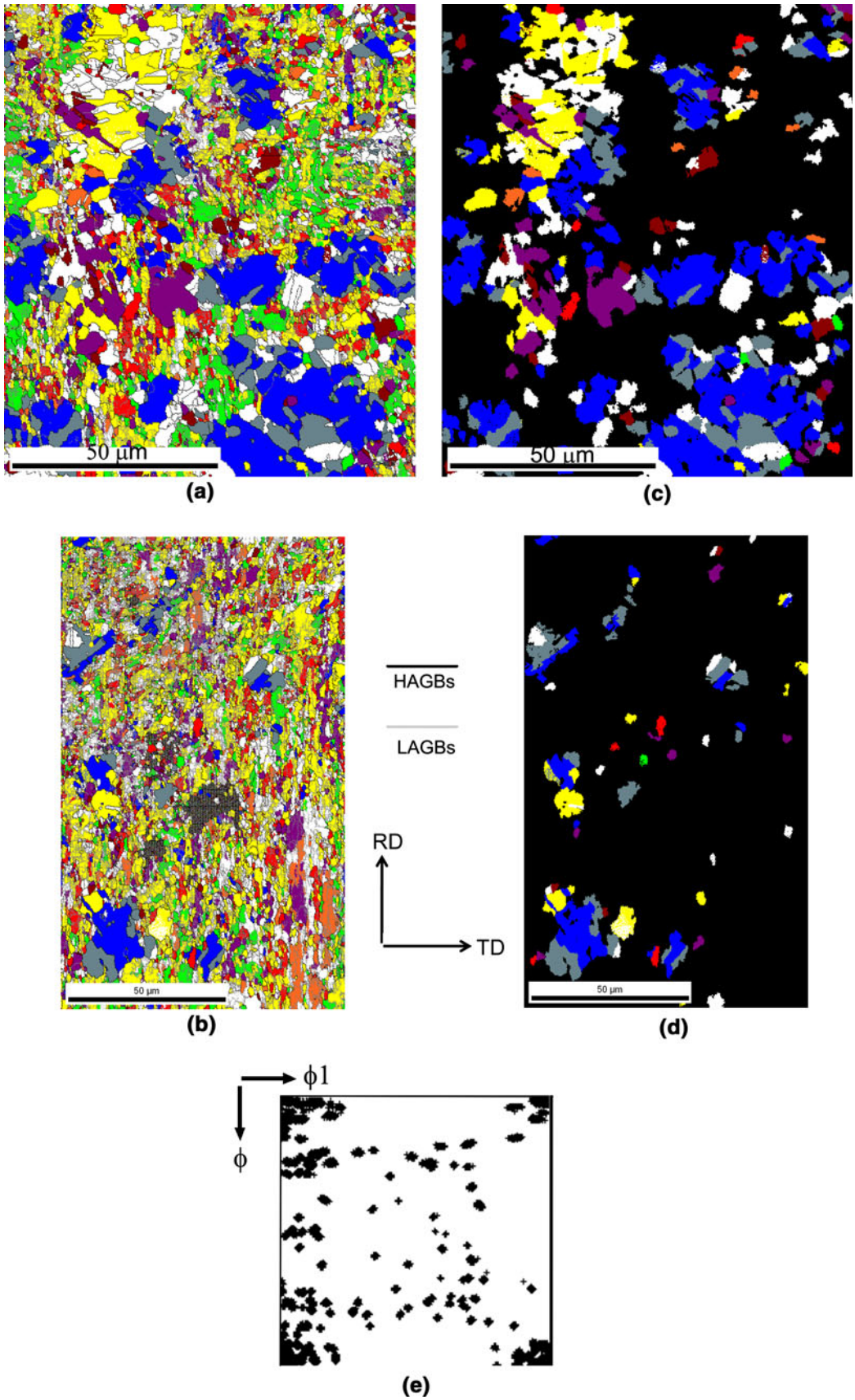

Fig. 14—(*a*) and (*b*) are orientation maps of ~95 pct cold-rolled Ni-W alloy after partial recrystallization at 973 K (700 °C) for 225 s; (*c*) and (*d*) are orientation maps showing the recrystallized fraction only. (*e*) is the $\Phi_2 = 0$ deg section of the discrete ODF plot compiled from the recrystallized fraction only of several orientation maps.

been observed in the current case, and thus, the observed preferential nucleation of cube (and rotated cube) grains seems to be primarily from the high-orientation gradient within the cube bands. Obviously, the much lower values of the orientation gradients (accumulated misorientations) encountered in the bands of orientations other than the cube bands precludes the chances of nucleation of grains of those orientations along with the cube (and rotated cube) grains during the early stages of recrystallization in both Ni and the Ni-W alloy. Although no direct (incontrovertible) proof has been provided that nucleation of cube (and rotated cube) grains actually does occur in the deformed cube bands, *in situ* nucleation studies, currently, are going on to find such direct evidence.

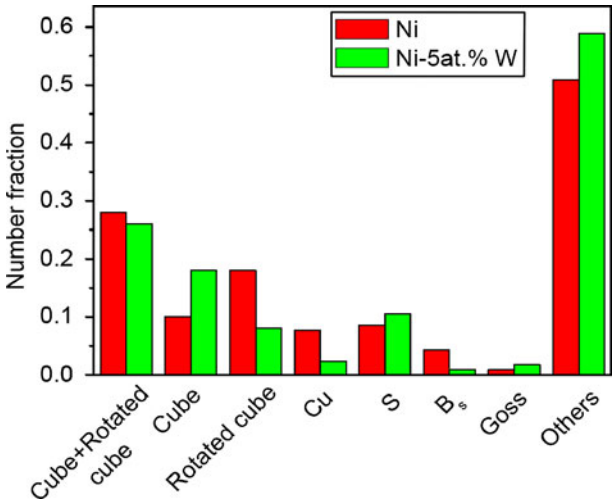

Fig. 15—Number fraction of grains of typical rolling texture orientations in high-purity Ni and Ni-W alloy at early stages of recrystallization.

A near cube and a rotated cube grain are related to each other by a low (~19 deg) misorientation angle. As a result, an advancing near cube grain finds it difficult to consume a neighboring rotated cube grain. This will restrict the growth of a near cube grain. More rotated cube than near cube grains nucleate in Ni at an early stage of recrystallization. Because chances of mutual impingement of these two orientations will be more here, the growth restriction of the near cube grains will be more effective in high-purity Ni. In the Ni-W alloy, because the fraction of rotated cube grains is lower initially compared with that in Ni, the cube volume fraction could increase considerably during the process of recrystallization.

Now the question that remains to be answered at this stage is why a larger number fraction of cube grains forms in the Ni-W alloy than in Ni at the early stages of recrystallization (Figure 15). From the same figure, it is clear that the number fraction of the cube plus the rotated cube grains in both Ni and the Ni-W alloy are comparable at this stage. This observation indicates that the effective number of nuclei of the cube plus the rotated cube grains is approximately similar in both Ni and the Ni-W alloy at the beginning of the recrystallization process.

Although the misorientation *vs* distance plots for the cube bands in both high-purity Ni and the Ni-W alloy (Figures 4 and 5) seem similar, there are some subtle differences also. Noteworthy among these is that

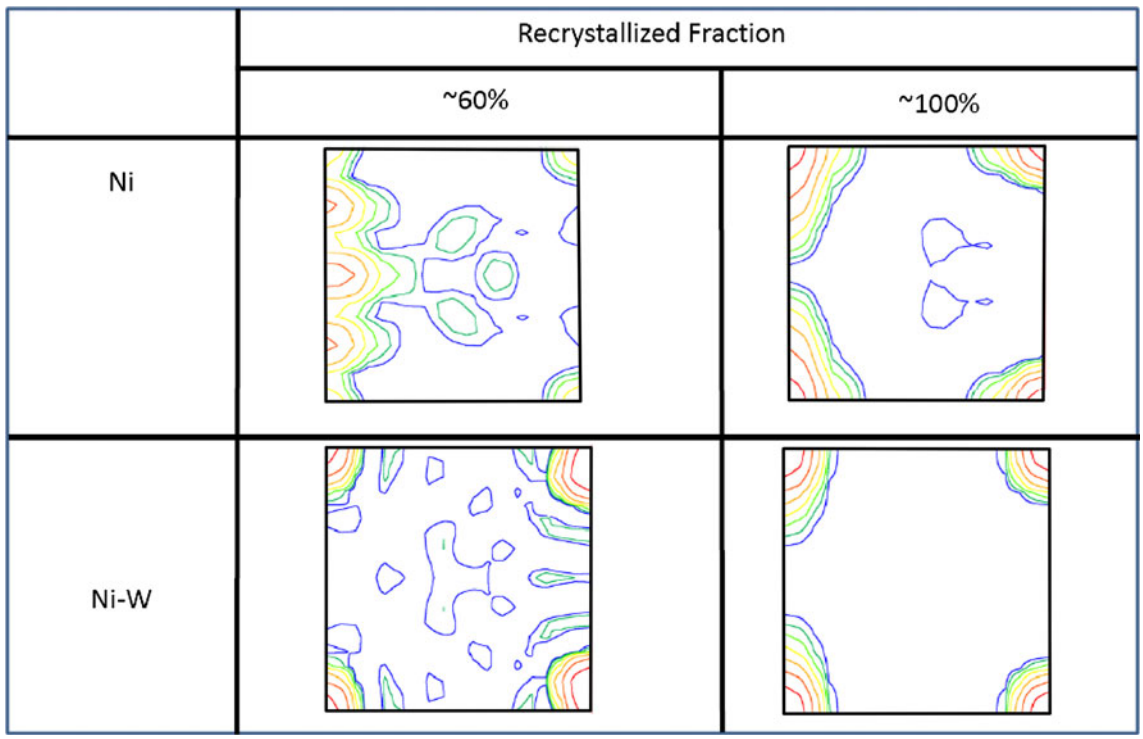

Fig. 16—Changes in the texture with progressing recrystallization in high-purity Ni and Ni-W alloy.

although for Ni, the misorientation angle increases monotonically with distance from the exact cube orientation, in the Ni-W alloy, this angle shows a sharp increase at a distance of 1 μm from the exact cube location then levels off and shows a decrease before increasing again. As a result, the rotated cube orientation (which is 19 deg away from the exact cube location) is encountered at a larger distance (6 μm) from the exact cube in the Ni-W alloy, whereas it lies at a shorter distance (5 μm) in Ni.

Using the calculations of Klein and Bunge,[16] Zaefferer *et al.*[15] have tried to explain how the orientation gradient forms within the cube bands during deformation. According to them, the cube orientation lies in a strongly diverging region of the orientation flow field. Using this concept, they have shown that the lattice rotation rate for the exact cube orientation is zero, whereas the rotation rate of an orientation (in the vicinity of the cube location) becomes larger as the orientation distance from the exact cube becomes larger. This conclusion also has been reached by Zhou *et al.*,[17] who used a rate-dependent crystal plasticity model.[18,19] The latter authors also have shown that a near cube orientation (Φ_1 = 1 deg, Φ = 1 deg, and Φ_2 = 89 deg) during deformation first will rotate to the alpha fiber (Goss—Brass), and then along alpha to beta (Brass—S—Taylor/Copper), and finally will be stabilized at a position near Taylor in the case of plain strain compression, or near copper in the case of relaxed constraints. Thus, it can be expected that during cold rolling of the sintered Ni and the Ni-W alloy, some amount of the remnant near cube-oriented volume (present in the sintered masses) will undergo lattice rotation, and some of the rotated volume will form the rotated cube orientation $\{013\}\langle 100\rangle$ (Φ_1 = 0 deg, Φ = 19 deg, and Φ_2 = 360 deg) on the way to forming the Goss orientation $\{011\}\langle 100\rangle$ (Φ_1 = 0 deg, Φ = 45 deg, and Φ_2 = 360 deg). This is possibly why the cube bands almost invariably show a range of orientations starting from near cube to rotated cube in the deformed Ni and the Ni-W alloy.

The distinctive difference in the misorientation *vs* distance (from exact cube) profiles of the cube bands in Ni and the Ni-W alloy may be explained as a result of the presence of W in the binary alloy. As shown by Bhattacharjee *et al.*[7] in the Ni-W alloy, W atoms are almost uniformly distributed throughout the matrix, with a slightly higher concentration in the grain boundaries. Because of the presence of the W atoms, it is expected that lattice rotation during deformation in the Ni-W alloy will be more difficult. It probably could be because dislocations of primary slip systems frequently are trapped by the solute W in the Ni-W alloy so that multiple slips (heterogeneous slip patterns) are activated more in the Ni-W alloy. This process will make the lattice rotations more difficult in the Ni-W alloy than in Ni, which will result in a significant decrease in the lattice rotation rate for orientations nearer to the exact cube orientation, for which the lattice rotation rate in any case is smaller. The effect of the W atoms on the lattice rotation rate of orientations further away from the exact cube will be minimal because for these orientations, the lattice rotation rate, in any case, is much larger. As a result, we get the typical misorientation–distance profile, as observed for the Ni-W alloy in which the misorientation regime is low for orientations closer to the exact cube followed by a much higher misorientation regime as we move further from the exact cube location. On the other hand, in the absence of the W atoms, as for Ni, the misorientation goes on increasing continuously as we move away from the exact cube location. Not only that, precisely for the same reason as stated earlier, the rotated cube orientation is obtained at a distance further away from the exact cube in the Ni-W alloy than in Ni,

In the Ni-W alloy, the misorientation–distance plot (Figure 5) shows practically zero misorientation for the near cube orientations lying at a range of distance (1 μm to 4.5 μm) from the exact cube. This essentially means that within the cube bands in the Ni-W alloy, several recovered cells or subgrains of near cube orientations have practically little misorientation between themselves and, therefore, can coarsen fast by the mechanism of subgrain coalescence, thereby becoming viable nuclei of near cube orientation with a size advantage ahead of the formation of the rotated cube nuclei. The extraordinarily strong Goss texture in Fe-Si alloys has been accounted for by invoking such a mechanism for the formation of the Goss-oriented grains.[20] The mechanism outlined can result in the strong near cube texture in the recrystallized Ni-W alloy. By contrast, in Ni, there will always be a competition between the near cube and the rotated cube nuclei to grow because of the continuous change in the misorientation existing between these two orientations. As a result, both rotated cube and near cube grains will coexist right from the early stages and prevail until the advanced stages of recrystallization. Finally, when the grains in the cube band start invading the surrounding matrix at a later stage, the near cube orientations, because of their faster growth rate,[1] will grow more than the rotated cube orientations, thereby making the cube texture component much stronger than the rotated cube. The stability of the rotated cube $\{013\}\langle 100\rangle$ grains, as has been observed in the course of the current investigation, also has been reported by Chang and Baker,[21] who have noticed this component to persist in Ni after annealing at different temperatures after a high deformation (98 pct).

The effect of the W atoms in the Ni-W alloy in modifying the texture becomes manifest during the stage of deformation of this alloy *vis à vis* high-purity Ni. As shown in Figure 2(c), although the cold-rolling textures of both Ni and Ni-W alloy seem similar qualitatively, the analysis of the volume fractions of the texture components in the two cases shows some characteristic differences. For example, all three major cold-rolling texture components, the copper, S, and brass show lower volume fractions in the Ni-W alloy compared with the situation in Ni. In fact, a host of extra orientations (written as others) appears in the texture of the cold-rolled Ni-W alloy. Hirsch and Lücke[22–24] thoroughly investigated the development of deformation texture in Al, Cu, and a host of Cu-Zn alloys. They observed that in medium-to-high stacking fault energy materials, like

Al and Cu, the strengths of the texture components copper, brass, and S increase continuously with an increasing deformation level. The fact that these components are somewhat weaker in the Ni-W alloy than in Ni indicates that lattice rotation might have been somewhat difficult in the presence of the W atoms in the Ni-W alloy. It is expected that the solid solution hardening caused by the addition of W may result in the restriction of glide in primary slip systems because of increased critical resolved shear stress for slip.

It may be recalled that the Ni-W alloy shows more deformation heterogeneities characterized by the presence of locally sheared regions than Ni (Figure 6). The presence of shear bands in the deformation microstructure usually is considered detrimental for the development of cube texture. This is a result of the nucleation of noncube or even random orientations in the shear banded regions in the process of recrystallization.[14,25,26] Clear evidence of nucleation of noncube-oriented grains has been reported in the locally sheared regions in this alloy.[27] However, the volume of sheared material either is limited, or sometimes the shear bands are not so well developed as observed in the current case. Thus, their effect on the development of cube texture seems to be limited.

V. CONCLUSIONS

1. The macroscopic deformation textures of high-purity Ni and the Ni-W alloy are typically pure metal or Cu type.
2. The deformation structures of the two materials are of lamellar type structure. Cube-oriented regions are present in thin bands elongated along the RD.
3. The long cube bands usually possess a high-orientation gradient from one end of the band to the other. This could be from the rotation of the cube-oriented cells about RD, thereby giving rise to the RD-rotated cube or $\{013\}\langle 100\rangle$ orientation.
4. After annealing at lower temperatures, a diffuse cube texture characterized by the development of the $\{013\}\langle 100\rangle$ component along with the cube component is observed in the two materials. The $\{013\}\langle 100\rangle$ component is much stronger in high-purity Ni than in the Ni-W alloy.
5. Annealing at higher temperatures strengthens the cube texture considerably in the Ni-W alloy. However, a strong RD-rotated cube component is retained in high-purity Ni.
6. The early recrystallized grains in high-purity Ni mostly have the rotated cube orientation. In contrast, more near cube grains are observed in the Ni-W alloy. The rotated cube grains nucleated during the early stages of recrystallization in high-purity Ni may exert a pinning effect on the growth of the cube grains because of the low misorientation angle between the two orientations. As a result, the cube component increases slowly in high-purity Ni. This could result in the observed difference in strength of the cube texture in the two materials after grain growth at higher annealing temperatures.
7. The total volume fraction of the near cube and the rotated cube grains during the early recrystallization stages are significantly higher compared with their miniscule presence in the deformation texture. This indicates a preferred nucleation of these orientations by an oriented nucleation mechanism.
8. The high-orientation gradient associated with the cube bands may offer a favorable nucleation environment that may result in preferential nucleation of the cube grains.

ACKNOWLEDGMENTS

The authors would like to acknowledge Dr. A. Upadhyaya, Associate Professor, IIT Kanpur, India for providing laboratory facilities for preparing the starting materials and Professor F. Wagner, LETAM, University of Metz, France for his kind permission to carry out the bulk texture measurement by XRD of several samples. P.P. Bhattacharjee would like to acknowledge the Japan Society for the Promotion Science (JSPS) for awarding a postdoctoral fellowship under the auspices of which part of this work has been carried out.

REFERENCES

1. R.D. Doherty, D.A. Hughes, F.J. Humphreys, J.J. Jonas, D.J. Jensen, M.E. Kassner, W.E. King, T.R. McNelley, H.J. McQueen, and A.D. Rollett: *Mater. Sci. Eng. A*, 1997, vol. 238, pp. 219–74.
2. I.L. Dillamore and H. Katoh: *Metal. Sci.*, 1974, vol. 8, pp. 73–83.
3. H.E. Vatne, R. Shahani, and E. Nes: *Acta Metall. Mater.*, 1996, vol. 44, pp. 4447–62.
4. H.E. Vatne, T. Furu, and E. Nes: *Mater. Sci. Technol.*, 1996, vol. 12, pp. 201–10.
5. A. Goyal, A.M.P. Paranthaman, and U. Schoop: *Mater. Res. Bull.*, 2004, vol. 29, pp. 552–61.
6. D. Dimos, P. Chaudhari, J. Mannhart, and F.K. Legoues: *Phys. Rev. Lett.*, 1988, vol. 61, pp. 219–22.
7. P.P. Bhattacharjee, R.K. Ray, and A. Upadhyaya: *Scripta Mater.*, 2005, vol. 53, pp. 1477–81.
8. K.T. Kim, J.H. Lim, J.H. Kim, S.H. Jang, J. Joo, C.J. Kim, K.J. Song, and H.S. Shin: *IEEE Appl. Supercon.*, 2005, vol. 15, pp. 2683–86.
9. H.J. Bunge: *Mathernatische Methoden der Textur-Analyse*, Academic Press, Berlin, Germany, 1969.
10. N. Hansen, D.J. Jensen, and T. Philos: *Roy. Soc. A*, 1999, vol. 357, pp. 1447–69.
11. D.A. Hughes and N. Hansen: *Philos. Mag.*, 2003, vol. 83, pp. 3871–93.
12. S. Wright and D.J. Field: *Advanced Software Capabilities for Automated EBSD*, Academic/Plenum Publishers, New York, NY, 2000.
13. X.L. Li, W. Liu, A. Godfrey, D.J. Jensen, and Q. Liu: *Acta Mater.*, 2007, vol. 55, pp. 3531–40.
14. A.A. Ridha and W.B. Hutchinson: *Acta Metall.*, 1982, vol. 30, pp. 1929–39.
15. S. Zaefferer, S.T. Baudin, and R. Penelle: *Acta Mater.*, 2001, vol. 49, pp. 1105–22.
16. H. Klein and H.J. Bunge: *Advances and Applications of Quantitative Texture Analysis*, Butterworths, London, UK, 1989.
17. Y. Zhou, L.S. Toth, and K.W. Neale: *Acta Metall. Mater.*, 1992, vol. 40, pp. 3179–93.
18. L.S. Toth, K.W. Neale, and J.J. Jonas: *Acta Metall. Mater.*, 1989, vol. 37, pp. 2197–2210.

19. K.W. Neale, L.S. Toth, and J.J. Jonas: *Int. J. Plast.*, 1990, vol. 6, pp. 45–61.
20. M. Matsuo: *ISIJ Int.*, 1989, vol. 29, pp. 809–27.
21. H. Chang and I. Baker: *Mater. Sci. Eng. A*, 2008, vol. 476, pp. 46–59.
22. J. Hirsch and K. Lucke: *Acta Metall. Mater.*, 1988, vol. 36, pp. 2863–82.
23. J. Hirsch and K. Lucke: *Acta Metall. Mater.*, 1988, vol. 36, pp. 2883–904.
24. J. Hirsch, K. Lucke, and M. Hatherly: *Acta Metall. Mater.*, 1988, vol. 36, pp. 2905–27.
25. T. Kamijo, H. Adachihara, and H. Fukutomi: *Acta Metall. Mater.*, 1993, vol. 41, pp. 975–85.
26. J. Hjelen, R. Orsund, and E. Nes: *Acta Metall. Mater.*, 1991, vol. 39, pp. 1377–1404.
27. P.P. Bhattacharjee, R.K. Ray, and N. Tsuji: *Acta Metall. Mater.*, 2009, vol. 57, pp. 2166–79.